

UCLA

UCLA Previously Published Works

Title

Capturing magnetic bead-based arrays using perpendicular magnetic anisotropy

Permalink

<https://escholarship.org/uc/item/0w33n21k>

Journal

Applied Physics Letters, 115(8)

ISSN

0003-6951

Authors

Hsiao, Yu-Ching

Khojah, Reem

Li, Xu

et al.

Publication Date

2019-08-19

DOI

10.1063/1.5085354

Peer reviewed

Published in final edited form as:
Appl Phys Lett. 2019 ; 115(8): .

Capturing magnetic bead-based arrays using perpendicular magnetic anisotropy

Yu-Ching Hsiao^{1,a}), Reem Khojah^{2,a}), Xu Li¹, Auni Kundu¹, Cai Chen¹, Daniel B. Gopman³, Andres C. Chavez¹, Taehwan Lee⁴, Zhuyun Xiao⁵, Abdon E. Sepulveda¹, Rob N. Candler^{1,5}, Gregory P. Carman¹, Dino Di Carlo^{1,2}, Christopher S. Lynch^{1,6,b})

¹Mechanical and Aerospace Engineering Department, University of California, Los Angeles, Los Angeles, California 90095, USA

²Bioengineering Department, University of California, Los Angeles, California 90095, USA

³Materials Science and Engineering Division, National Institute of Standards and Technology, Gaithersburg, Maryland 20899, USA

⁴Materials Science and Engineering Department, University of California, Los Angeles, Los Angeles, California 90095, USA

⁵Electrical and Computer Engineering Department, University of California, Los Angeles, California 90095, USA

⁶Bourns College of Engineering, University of California, Riverside, California 92521, USA

Abstract

Designing and implementing means of locally trapping magnetic beads and understanding the factors underlying the bead capture force are important steps toward advancing the capture-release process of magnetic particles for biological applications. In particular, capturing magnetically labeled cells using magnetic microstructures with perpendicular magnetic anisotropy (PMA) will enable an approach to cell manipulation for emerging lab-on-a-chip devices. Here, a Co (0.2 nm)/Ni (0.4 nm) multilayered structure was designed to exhibit strong PMA and large saturation magnetization (M_s). Finite element simulations were performed to assess the dependence of the capture force on the value of M_s . The simulated force profile indicated the largest force at the perimeter of the disks. Arrays of Co/Ni disk structures of (4–7) μm diameter were fabricated and tested in a microchannel with suspended fluorescent magnetic beads. The magnetic beads were captured and localized to the edge of the disks as predicted by the simulations. This approach has been demonstrated to enable uniform assembly of magnetic beads without external fields and may provide a pathway toward precise cell manipulation methods.

Disk arrays with perpendicular magnetic anisotropy (PMA) are designed, fabricated, and demonstrated to be capable of capturing micrometer scale magnetic beads suspended in a fluid.¹ They have the potential to enable lab-on-a-chip cell manipulation devices.^{2,3} Magnetic bead-based methods have facilitated many biomedical applications including

^b) Author to whom correspondence should be addressed: cslynch@engr.ucl.edu.

^a) Contributions: Yu.-C. Hsiao and R. Khojah contributed equally to this work.

biochemical detection,⁴ nucleic acid extraction,⁵ and cell separation and manipulation.⁶ Magnetic bead-based cell capture platforms have the advantage of allowing functionalized magnetic beads to bind and target cells in solution. Target cells are separated from suspension using the external magnetic field from hard permanent magnets. However, the large external magnetic field leads cells to aggregate to one location in the reaction chamber, leaving limited space for imaging and analysis to quantify different analytes simultaneously.⁷ External magnetic field-based systems cannot currently assemble micromagnetic beads uniformly in arrays to allow detection and analysis in microfluidic devices. Thus, precise localization of magnetic beads at the microscale is needed for precise cell localization.

This study demonstrates magnetic bead assembly in a uniform array using the magnetic force produced by disk shaped heterostructures displaying PMA.⁸ PMA describes the case where the easy axis of magnetization is perpendicular to the plane of the heterostructure or film. This effect occurs in certain ultrathin film systems and at the interface of multilayers.^{9,10} Co/Ni multilayers were selected for their large PMA compared to other Cocontaining multilayers such as Co/Ag and Co/Au.^{1,11} Anisotropy energy and saturation magnetization (M_s) can be adjusted by modification of the relative thickness of the layers.¹² In comparison to other methods,^{13–18} this PMA assisted capture method does not require external fields or other energy supplied, simplifying its use. Heterostructures with PMA generate a magnetic gradient in their vicinity that acts on the magnetic beads. In this approach, the majority of beads are trapped on the disk perimeter.

A numerical model was used to understand the distribution of bead trapping force on the Co/Ni disk as well as changes in bead capture force due to varying M_s values of the Co/Ni disk.^{19–21} A finite element approach was used to simulate the magnetic field distribution around the Co/Ni disk and its interactions with a magnetic bead. The thickness of Co/Ni was set at 4 nm, and uniform out-of-plane (OOP) magnetization with magnitude M_s was initialized within the disk, resulting in a magnetic field exterior to the disk. Out-of-plane initialization of magnetization duplicates the PMA effect. The magnetic force components on the bead were calculated at different spatial positions within this field using the finite element simulations together with Eqs. (1)–(4). The calculated magnetic field distribution was used with post processing to determine the bead capture force.

The capture force was calculated using the following equation:

$$F_{bead} = -\nabla U, \quad (1)$$

where F_{bead} is the capture force of the bead.

The total magnetic potential energy (U) is an integration of magnetic energy density (u) over the bead volume, given as follows:

$$U = \iiint_V u dV. \quad (2)$$

The energy density was determined using the following equation:

$$u = -M \cdot B, \quad (3)$$

where M is the induced magnetization in the magnetic bead and B is the magnetic flux generated in the bead by the Co/Ni disk. The relation between B and M is expressed by the following equation:

$$B = \mu_0 \left(1 + \frac{1}{\chi_m} \right) M, \quad (4)$$

where μ_0 is the vacuum permeability; χ_m is the magnetic susceptibility.^{22,23} From Eqs. (1)–(4), it is found that the capture force is related to the bead volume and magnetic flux generated from the Co/Ni disk, proportional to M_s^2 of the Co/Ni disk.

For the simulations, the bead position was varied from coincident with the disk center to a $-3 \mu\text{m}$ horizontal displacement in 500nm increments. Since the magnetic force is spatially symmetric, calculations were only performed for one half of the disk. The net force was calculated for a series of bead diameters and M_s values of a prospective Co/Ni disk. Specifically, five values of M_s , {600, 700, 800, 900, 1000} kA/m, were selected. These choices were made because they span the possible range of expected M_s values for Co/Ni multilayers. The bulk M_s values of Co and Ni are 1400kA/m and 490kA/m,^{24,25} respectively, and can be achieved by varying the relative layer thickness. Each M_s value was tested with four different bead diameters of {0.2, 0.4, 0.6, 0.8} μm . These bead diameters were chosen because smaller magnetic beads provide a higher spatial resolution when imaging the distribution of the magnetic beads in the testing section. A 4 μm diameter Co/Ni disk was used in all simulations.

The simulated capture force vs bead location profile for one combination of parameters is presented in Fig. 1(a). This shows the results for a Co/Ni disk with an M_s value of 800 (kA/m) and a bead diameter of 0.8 (μm). The capture force rises as the bead is moved from the left side toward the center of the disk and reaches a peak value at the disk edge (i.e., $x = -2 \mu\text{m}$). The force falls as the bead location is moved further to the right and approaches the center of the Co/Ni disk. The maximum net force occurs at the disk edge where the largest magnetic flux gradient from the disk is generated.

The maximum force as a function of bead diameter at various M_s values is illustrated in Fig. 1(b). The plot shows that maximum force does not change significantly with the bead diameter, which provides flexibility in choosing the nanomagnetic bead size. This can be explained by recognizing that the magnetic field from the Co/Ni disk is localized to the edge causing a magnetization gradient in the bead. Consequently, the magnetized volume does not significantly change even with the increasing bead diameter. In contrast, the capture forces show a high dependence on the value of M_s , which proves that the magnetic flux is proportional to M_s of the Co/Ni disk. For example, the maximum force increases ~ 2 times when increasing the M_s value from 700kA/m to 1000kA/m. The advantage of using a multilayer structure is that the relative thickness between Co and Ni films is readily tunable. Hence, it is experimentally possible to modify the maximum capture force by tuning M_s of the Co/Ni multilayers.

Simulation results indicate that high M_s yields larger trapping force on the bead. This can be achieved via a high Co to Ni ratio. However, overly large Co to Ni ratio risks losing PMA.^{12,26,27} A Co (0.2nm)/Ni (0.4nm) structure was selected for its relatively high M_s while maintaining stable perpendicular magnetization. This structure was produced on a 0.5 mm thick single crystalline Si (001) substrate by e-beam evaporation^{28,29} at room temperature with a base pressure of 2×10^{-6} Torr. The substrate was cleaned with acetone, methanol, and isopropanol, followed by one-minute O₂ plasma cleaning (80 W *rf* power, 3.75 Torr, 50°C) prior to the deposition process. Four repeated Co (0.2 nm)/Ni (0.4nm) layers were grown on top of a Pt (3 nm) buffer layer and a Ti (2 nm) adhesion layer. Pt was chosen as the seed layer because it has been experimentally demonstrated to enhance the PMA in Co/Ni multilayers.³⁰ Ti was chosen to improve adhesion of Pt to the substrate. For symmetry, an extra Co layer (0.2 nm) was deposited on top of Co/Ni multilayers. The entire structure was then capped by a Pt (3 nm) layer to prevent metal oxidation. Disks with 4 μm –7 μm diameters and 12 μm separation between the centers of disks were patterned by a lift-off method using photoresist nLof2020. A simulation was performed to understand the effect of burrs at the edge of the disk caused by the lift-off process. The results show that the edge imperfection associated with lift-off methods does not impact the capture force on magnetic beads significantly.

To benchmark the relevant M_s of this heterostructure, a full film sample was characterized using a Superconducting Quantum Interference Device (SQUID) in the DC mode. The presence of an out-of-plane easy axis consistent with PMA is confirmed in the hysteresis loop shown in Fig. 2. The out-of-plane (OOP) curve has a much lower saturation field and higher magnetic remanence than the inplane (IP) curve. Furthermore, experimental values of OOP M_s (870 kA/m) and IP (860 kA/m) are consistent with the theoretical value of 840 kA/m, which was obtained from the Co/Ni thickness ratio (1: 1.6) by the rule of mixtures. This confirms that the desired M_s was obtained by growing a film with the relevant Co to Ni thickness ratio.

The structure was next tested for trapping fluorescent beads using a microchannel. A microfluidic device was integrated with the Co/Ni disks, and fluorescent magnetic beads were passed through the device and imaged using a fluorescent microscope to observe the magnetic bead capture events. The disk array is shown in Fig. 3(a). The microfluidic channel and surfaces of microstructures were passivated with a surfactant to prevent nonspecific surface interactions of the magnetic beads. The details of materials and methods are described in the supplementary material. Magnetic beads were localized on the Co/Ni micropattern array as shown in Fig. 3(b). To provide further evidence to support bead-based capture via PMA, the disk arrays were partially covered with a polydimethylsiloxane (PDMS) layer of 1mm thickness prior to introducing the magnetic beads in suspension. The beads were not captured by PDMS covered disks, Fig. 3(c).

The PMA field capture and localization were characterized by tracking magnetic bead binding sites on the surface of Co/Ni disks. Micromagnetic beads (diameter = 2.8 μm) labeled with red fluorescent dye in fluid were introduced to Co/Ni disks (diameter = 7 μm). Magnetic binding locations were observed on the edges of the Co/Ni disks [Fig. 3(d)]. Specifically, micromagnetic beads were equally distributed and localized at different angles

(θ) from the center of each disk. This indicates a large magnetic field gradient associated with the magnetization field produced on the perimeter of Co/Ni disks as suggested by the simulations.

Smaller magnetic beads were used to increase the spatial resolution when imaging magnetic beads. The fluorescent nanomagnetic particles (diameter = 400 nm–500 nm) were captured on the previously tested Co/Ni disks (diameter = 7 μm) [Fig. 4(a)]. Quantitative measurements of nanomagnetic bead localization were made by image analysis of the fluorescence intensity (grayscale) around the Co/Ni disks. An overlay image of the disks was generated, where pixels with a fluorescence signal corresponds to the location of nanomagnetic beads [Fig. 4(b)]. The image intensity map is collected from each disk and then averaged over a population of 50 Co/Ni disks within the array. The magnetic capture spatial distribution map confirms that the most effective magnetic trapping region coincides with the region of the maximal magnetic field gradient at the perimeter of Co/Ni disks [Fig. 4(c)].

In this study, multilayered Co/Ni disk arrays exhibiting PMA were designed, fabricated, and demonstrated to capture magnetic beads. Finite element simulations indicate that different M_s values, which can be modified by varying the relative Co/Ni thickness ratio, significantly change the magnetic capture forces. Based on the modeling results, a Co (0.2 nm)/Ni (0.4 nm) multilayered structure was selected due to its OOP easy axis and relatively large PMA. Patterned Co/Ni disks were tested in a suspension of fluorescent magnetic beads in fluid, showing that the perimeter of disks trapped most of the magnetic beads. This observation agreed with the modeling results that the maximum capture force occurs at the edge of the disk. By eliminating the need for an externally applied field, this approach to magnetic bead capture provides a promising pathway toward compact lab-on-a-chip devices for more precise cell manipulation.

See the supplementary material for the device setup & imaging and analysis.

Supplementary Material

Refer to Web version on PubMed Central for supplementary material.

Acknowledgments

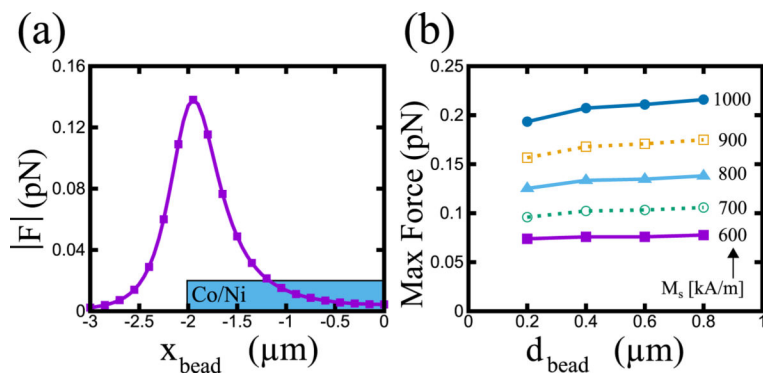
This work was supported by the NSF Nanosystems Engineering Research Center for Translational Applications of Nanoscale Multiferroic Systems (TANMS) under the Cooperative Agreement Award No. EEC-1160504.

REFERENCES

1. Johnson M, Bloemen P, Broeder F, and Vries J, "Magnetic anisotropy in metallic multilayers," Rep. Prog. Phys. 59(11), 1409–1458 (1996).
2. Medoro G, Manaresi N, Leonardi A, Altomare L, Tartagni M, and Guerrieri R, "A lab-on-a-chip for cell detection and manipulation," IEEE Sens. J. 3(3), 317–325 (2003).
3. Xiao Z, Khojah R, Chooljian M, Lo Conte R, Schneider JD, Fitzell K, Chopdekar RV, Wang Y, Scholl A, Chang J, Carman GP, Bokor J, Di Carlo D, and Candler RN, "Cytocompatible magnetostrictive microstructures for nano- and microparticle manipulation on linear strain response piezoelectrics," Multifunct. Mater. 1(1), 014004 (2018).

4. Choi J-W, Oh KW, Thomas JH, Heineman WR, Halsall HB, Nevin JH, Helmicki AJ, Henderson HT, and Ahn CH, "An integrated microfluidic biochemical detection system for protein analysis with magnetic bead-based sampling capabilities," *Lab Chip* 2(1), 27 (2002). [PubMed: 15100857]
5. Berensmeier S, "Magnetic particles for the separation and purification of nucleic acids," *Appl. Microbiol. Biotechnol.* 73(3), 495–504 (2006). [PubMed: 17063328]
6. Adams JD, Kim U, and Soh HT, "Multitarget magnetic activated cell sorter," *Proc. Natl. Acad. Sci. U. S. A.* 105(47), 18165–18170 (2008).
7. Pamme N, "Magnetism and microfluidics," *Lab Chip* 6(1), 24–38 (2006). [PubMed: 16372066]
8. den Broeder FJA, Hoving W, and Bloemen PJH, "Magnetic anisotropy of multilayers," *J. Magn. Magn. Mater.* 93, 562–570 (1991).
9. Bochi G, Ballentine CA, Inglefield HE, Thompson CV, O'handley RC, Hug HJ, Stiefel B, Moser A, and Güntherodt H-J, "Perpendicular magnetic anisotropy, domains, and misfit strain in epitaxial Ni/Cu 1-x Ni x/Cu/Si (001) thin films," *Phys. Rev. B* 52(10), 7311–7321 (1995).
10. Beaujour J-ML, Chen W, Krycka K, Kao C-C, Sun JZ, and Kent AD, "Ferromagnetic resonance study of sputtered Co/Ni multilayers," *Eur. Phys. J.B* 59, 475–483 (2007).
11. Sbiaa R, Meng H, and Piramanayagam SN, "Materials with perpendicular magnetic anisotropy for magnetic random access memory," *Phys. Status Solidi RRL.* 5(12), 413–419 (2011).
12. Gopman DB, Dennis CL, Chen PJ, Iunin YL, Finkel P, Staruch M, and Shull RD, "Strain-assisted magnetization reversal in Co/Ni multilayers with perpendicular magnetic anisotropy," *Sci. Rep.* 6(1), 27774 (2016).
13. Hultgren A, Tanase M, Chen CS, Meyer GJ, and Reich DH, "Cell manipulation using magnetic nanowires," *Cit. J. Appl. Phys.* 93, 7554 (2003).
14. Yun H, Kim K, and Lee WG, "Cell manipulation in microfluidics," *Biofabrication* 5(2), 022001. (2013).
15. Voldman J, "Electrical forces for Microscale cell manipulation," *Annu. Rev. Biomed. Eng.* 8(1), 425–454 (2006). [PubMed: 16834563]
16. Ashkin A and Dziedzic JM, "Internal cell manipulation using infrared laser traps," *Proc. Natl. Acad. Sci. U. S. A.* 86(20), 7914–7918 (1989). [PubMed: 2813368]
17. Tokura Y, "Multiferroics—toward strong coupling between magnetization and polarization in a solid," *J. Magn. Magn. Mater.* 310(2), 1145–1150 (2007).
18. Liu C, Stakenborg T, Peeters S, and Lagae L, "Cell manipulation with magnetic particles toward microfluidic cytometry," *J. Appl. Phys.* 105(10), 102014 (2009).
19. Liang C-Y, Keller SM, Sepulveda AE, Bur A, Sun W-Y, Wetzlar K, and Carman GP, "Modeling of magnetoelastic nanostructures with a fully coupled mechanical-micromagnetic model," *Nanotechnol.* 25(43), 435701 (2014).
20. Barra A, Mal A, Carman G, and Sepulveda A, "Voltage induced mechanical/spin wave propagation over long distances," *Appl. Phys. Lett.* 110(7), 072401 (2017).
21. Xiao Z, Conte RL, Chen C, Liang C-Y, Sepulveda A, Bokor J, Carman GP, and Candler RN, "Bi-directional coupling in strain-mediated multiferroic heterostructures with magnetic domains and domain wall motion," *Sci. Rep.*, 8(1), 5207 (2018). [PubMed: 29581531]
22. Rapoport E and Beach GS, "Magneto-mechanical resonance of a single superparamagnetic microbead trapped by a magnetic domain wall," *J. Appl. Phys* 111(7), 07B310 (2012).
23. Chen P, Huang YY, Hoshino K, and Zhang JX, "Microscale magnetic field modulation for enhanced capture and distribution of rare circulating tumor cells," *Sci. Rep.* 5, 8745 (2015). [PubMed: 25735563]
24. Crangle J and Goodman GM, "The magnetization of pure iron and nickel," *Proc. R. Soc. London. A. Math. Phys. Sci.* 321(1547), 477–491 (1971).
25. Kneller EF and Hawig R, "The exchange-spring magnet: A new material principle for permanent magnets," *IEEE Trans. Magn.* 27(4), 3588–3560 (1991).
26. Kittel C, "On the Theory of Ferromagnetic Resonance Absorption," *Phys. Rev.* 73(2), 155–161 (1948).

27. Daalderop GHO, Kelly PJ, and Den Broeder FJA, "Prediction and confirmation of perpendicular magnetic anisotropy in Co/Ni multilayers," *Phys. Rev. Lett.* 68(5), 682–685 (1992). [PubMed: 10045963]
28. Mangin S, Ravelosona D, Katine JA, Carey MJ, Terris BD, and Fullerton EE, "Current-induced magnetization reversal in nanopillars with perpendicular anisotropy," *Nat. Mater.* 5(3), 210–215 (2006).
29. Gottwald M, Andrieu S, Gimbert F, Shipton E, Calmels L, Magen C, Snoeck E, Liberati M, Hauet T, Arenholz E, Mangin S, and Fullerton EE, "Co/Ni(111) superlattices studied by microscopy, x-ray absorption, and ab initio calculations," *Phys. Rev. B* 86(1), p. 014425 (2012).
30. Nakajima N, Koide T, Shidara T, Miyauchi H, Fukutani H, Fujimori A, Iio K, Katayama T, Nývlt M, and Suzuki Y, "Perpendicular Magnetic Anisotropy Caused by Interfacial Hybridization via Enhanced Orbital Moment in Co/Pt Multilayers: Magnetic Circular X-Ray Dichroism Study," *Phys. Rev. Lett.* 81(23), 5229–5232 (1998).

**FIG. 1.**

(a) Force on a magnetic bead ($0.8 \mu\text{m}$ diameter) when placed at different locations. The blue box indicates the half side of the Co/Ni disk. (b) Maximum force determined from different M_s values of the Co/Ni disk as a function of each bead diameter. The maximum capture forces for (b) were extracted from the peak value of the corresponding force profile similar to the one shown in (a).

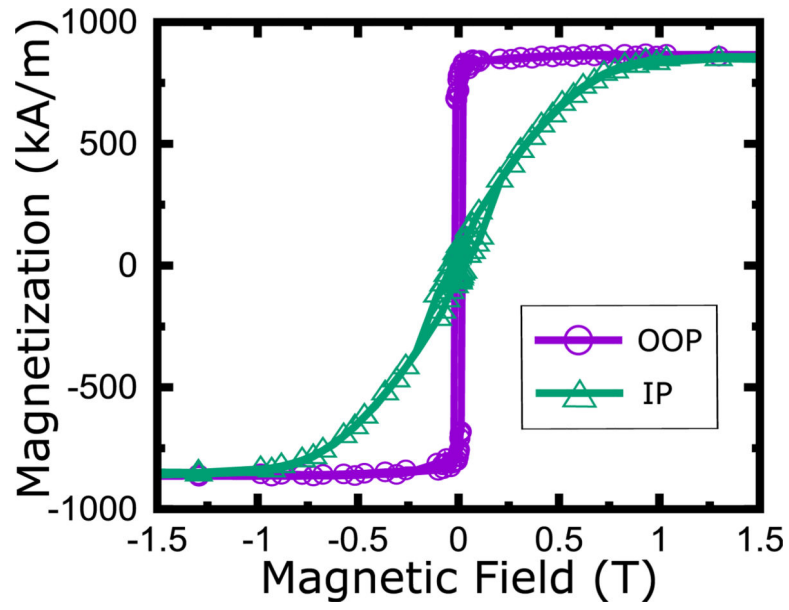
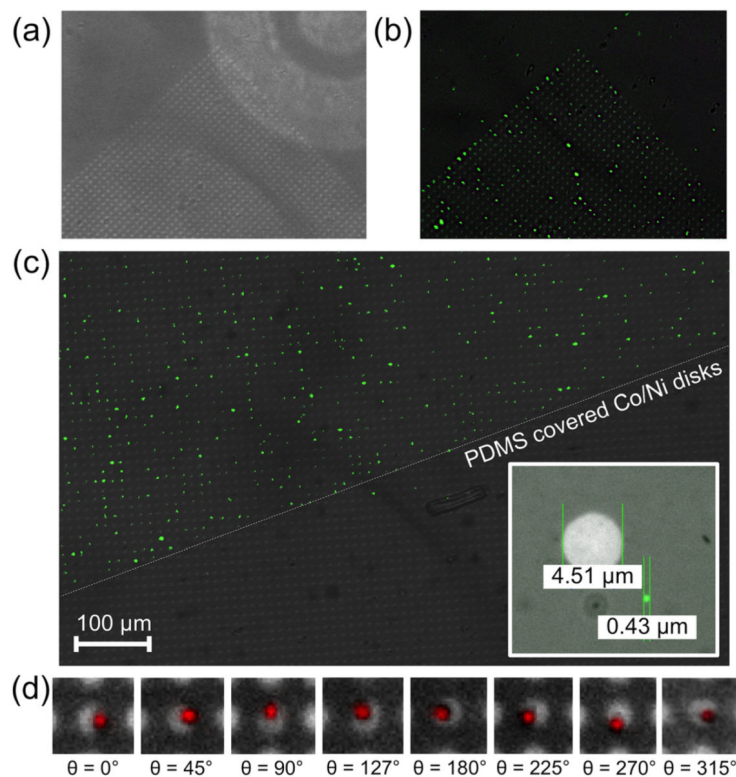


FIG. 2. Magnetization vs applied field hysteresis loop for a full film Co (0.2 nm)/Ni (0.4 nm) heterostructure under inplane (IP) and out-of-plane (OOP) applied fields.

**FIG. 3.**

Co/Ni multilayer disks (diameter = $4.5 \mu\text{m}$) with PMA demonstrate the high capture rate of magnetic beads labeled with green fluorescence (diameter = $0.4 \mu\text{m}$). (a) Bright field image of Co/Ni multilayer disks before passing fluorescent magnetic beads. (b) Overlay of bright field and fluorescence images of magnetic beads on the Co/Ni disk array demonstrates localized capture. (c) Partially covered substrate with the PDMS layer shows selective binding and localization of fluid-born beads on Co/Ni multilayer disks. (d) The location of magnetic bead-binding events at different angles (θ) with the polar coordinate system chosen at (1,0) on the circular surface of the Co/Ni microdisks.

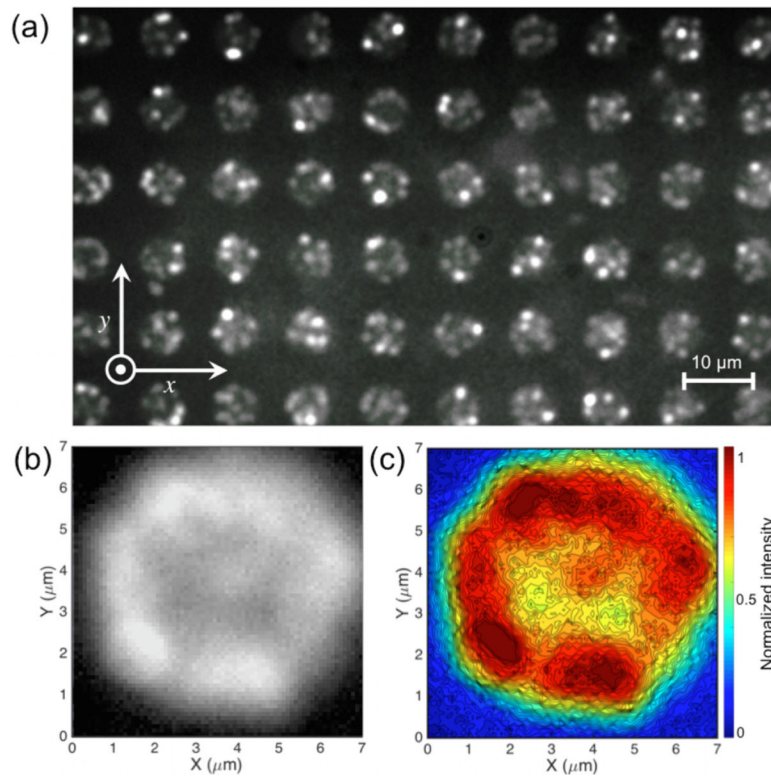


FIG. 4. Quantitative image analysis of nanomagnetic bead distribution on the surface of Co/Ni disks. (a) Fluorescence microscopy image of nanomagnetic capture and build-up on $7\ \mu\text{m}$ Co/Ni disks. (b) Fluorescence intensity of an image overlay of Co/Ni disks (c) Normalized intensity map of the image overlay show the high magnetic trapping region on the perimeter of Co/Ni disks.